DYNAMICS OF TEMPERING PROCESSES IN STAINLESS STEEL

LEO T. H. DE JEER, VÁCLAV OCELÍK & JEFF TH. M. DE HOSSON
Department of Applied Physics, University of Groningen, The Netherlands

ABSTRACT

In this study, we focused on the dynamics of the continuously changing microstructure at an elevated temperature upon tempering of stainless steel. We used a Scanning Electron Microscope (SEM) with an Electron Backscatter Diffraction (EBSD) setup in combination with a High Temperature specimen stage to perform in-situ orientation imaging microscopy experiments. This experimental setup allowed us to observe in-situ the microstructural changes like grain growth, grain-boundary movement and modification in crystal orientations. By subsequent imaging of the outer surface area, the evolution of the microstructure can be examined leading to a better understanding of the dynamics of the tempering process of stainless steel. In particular, we discussed the results obtained of the microstructural changes at a fixed temperature of 500°C. A loss of the EBSD signal started at the triple junctions and at high angle grain boundaries over time and is attributed to oxidation. We concluded that preferred oxidation occurs during treatment and that dynamic in situ observations are possible.

Keywords: electron backscatter diffraction, high temperature, stainless steel, microstructure, tempering.

1 INTRODUCTION

The behavior at the surface of materials during tempering is an old, but still active subject of research and holds a large interest in the manufacturing industry for optimizing industrial processes. Especially where a high degree of control of the surface processes is of key importance for the quality of products. In the high tech industry, there is a need for high quality and high precision materials. Components in the devices not only need to become smaller but also need the appropriate bulk and surface properties. To this end martensitic stainless steel finds its way in many household applications: ranging from house hold cutlery to parts of electrical shavers.

At temperatures around 1/3 of the melting temperature, recovery processes take place at temperatures just before recrystallization [1]. These processes involve the release of residual stresses introduced by various production process steps, e.g. cold rolling. Due to elevated temperature, the dislocations can glide and climb to the surface and grain boundaries. This usually is visible in the microstructure by a more homogenous orientation distribution within a grain, i.e. less crystallographic misorientation.

Next to recovery of the material an oxidation on the surface will occur during tempering of the stainless steel. The oxidation process at the surface is in particular relevant for the corrosion resistance of stainless steel [2]–[4]. Several high temperature experimental methods exist to explore the mechanisms behind surface oxidation. A couple of attempts combining high temperature and optical microscopy were performed for example on Fe-C [5]. For steel, oxidation at temperatures above the recovery temperature, i.e. T~1000 °C, are usually done [5], [6]. For martensitic stainless steel, usually the tempering behavior after hardening of martensitic steel is studied [7], [8]. However, scant literature exists on the effect of the microstructure on the oxidation process on stainless steel at recovery temperatures.

WIT Transactions on Engineering Sciences, Vol 116, © 2017 WIT Press
www.witpress.com, ISSN 1746-4471 (on-line)
doi:10.2495/MC170191

In this study, we correlate the microstructural changes on the surface of stainless steel to the oxidation behavior. The novelty of this experiment is that we observe in-situ the effect of oxidation at an elevated temperature in combination with the change of the microstructure using Electron Backscattered Diffraction.

2 METHOD & MATERIALS

The as received material is a cold rolled sheet of martensitic stainless steel (MSS) in the ferritic state. The material was rolled into sheets with thickness of 0.45 mm at the manufacturer. For sample preparation, the samples of 1x1 cm^2 were cut out of the sheet with an abrasive saw. The samples were mechanically polished up to 0.04 μm sized particles for EBSD analysis.

The High Temperature (HT) Experiments were performed in a Scanning Electron Microscope (SEM) (FEG TESCAN, Czech Republic) environmental pressure (10^{-6} bar) in combination with a Heating Module specimen stage (Kammrath & Weiss GmbH, Germany). Electron Backscattered Diffraction (EBSD) (Edax Inc., Draper, Utah, USA) was used for the crystallographic characterization and Energy Dispersive X-ray Spectroscopy (EDS) (Edax Inc., Draper, Utah, USA) was used for the elemental characterization.

The MSS was heated up with a rate of 35°C/min up to 500°C. The tempering time was 90 min at a fixed temperature of 500°C. During the tempering in situ EBSD scans were made of a selected area. By scanning the same area for whole duration of the experiment the microstructural and crystallographic orientation changes were tracked. The selected area of 20x20 μm^2 was scanned in a hexagonal grid with a step size of 0.4 μm. Each scan took 2 minutes to complete. EBSD data were analyzed by using the OIM Analysis 7.3 software.

3 RESULTS

The composition of the MSS was measured with EDS. The MSS consist of 13% Cr and 0.2% C and some minor traces of Si, Mn, P and S, see Table 1. The general microstructure consists of ferrite grains of ~10 μm in diameter and $Cr_{23}C_6$ chromium carbides of ~1 μm in diameter. The majority of the chromium carbides reside intergranular on grain boundaries and triple points, but some intragranular chromium carbides are also observed. The microstructures of the selected area at the onset, during and at the end of the 500 °C tempering process are shown in Fig. 1. The local average misorientation (LAM) values in Fig. 1 clearly show an increase with respect to the start. Also, the number of non-indexed points increases. Due to the prior cold rolling process, the material is highly textured, i.e. has an inhomogeneous crystallographic orientation distribution,

The heat treatment causes an increase of misorientation and therefore strain at the surface. In Fig. 2 the distribution of kernel average misorientation (KAM), with which we calculate the misorientation at a certain distance, for different times is plotted. The change in distribution of the short-range strain is plotted in Fig. 2(a) where the misorientation with respect to the 1st nearest neighbor is used. The shift in distribution shows a continuous

Table 1: Composition of the martensitic stainless steel as measured by EDS.

	C	Si	Mn	P	S	Cr	Fe
At %	0.16-0.40	<1.00	<1.00	<0.040	<0.030	12.0-14.0	Bal.

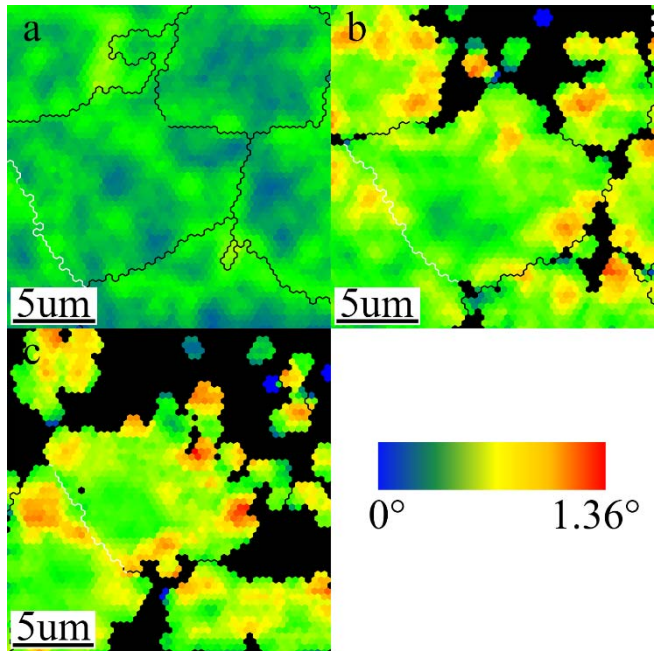

Figure 1: Microstructure of the stainless steel with 2nd order local average misorientation (LAM) maps superimposed over it. (a) Map at t=0 min; (b) Map at t=56 min; (c) Map at t=90 min. Black points are non-indexed points due to oxidation. The white lines correspond to low angle grain boundaries (5°–15°) and the black lines correspond to high angle grain boundaries (>15°). Visible is that the LAM is significantly increased during tempering and an increase in number of non-indexed points.

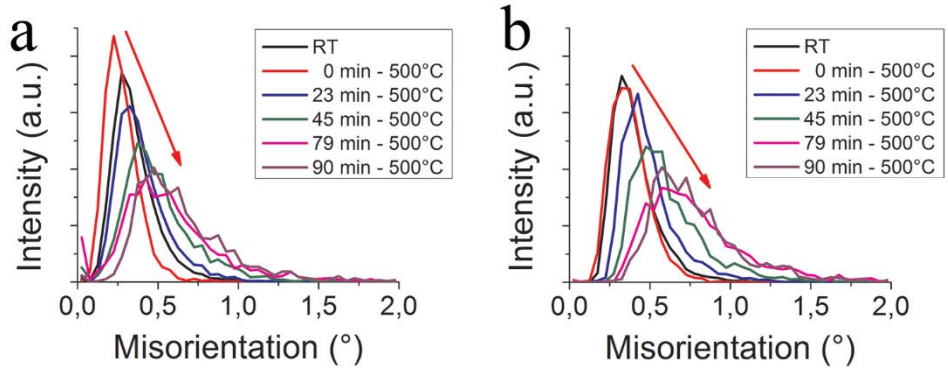

Figure 2: Increase of Kernel Average Misorientation with time at a constant temperature of 500°C. An increase of KAM is observed despite the recovery process. This holds for both (a) the short range (1st neighbor) as well as (b) the long range (3rd neighbor). The surface is therefore more strained after the tempering procedure.

increase in the KAM average and widening of the KAM distribution. The same holds for the distributions of the long-range strain, Fig. 2b, where the misorientation with respect to the 3rd nearest neighbor is shown. The high KAM values are mostly found at the grain boundaries and triple junctions.

During the tempering process at 500 °C a gradual loss of Kikuchi pattern was observed. In Fig. 3 the non-indexed sample surface fraction is plotted versus time. A point is considered non-indexed if the probability of proper indexing is smaller than 0.9. The plot shows a fast increase in number of non-indexed points after 30 minutes and a reduced increase at the end of the experiment.

After tempering the surface of the MSS sample was oxidized, see Fig. 4. The different colors denote the different thickness of oxide layer. A distinct appearance between the covered part and the non-covered part can be seen. The right non-covered part is light blue and has the thickest oxide layer. The left covered part is white to dark blue depending on the degree of oxidation on the surface. After cooling EBSD scans have been performed on areas with different colors. At the white areas with a thin oxide layer a good Kikuchi pattern was still obtained. Contrary at the blue areas with a thick oxide layer no Kikuchi pattern was obtained. We therefore hypothesize that the oxide layer is a major contributor for the loss of Kikuchi pattern during the in-situ HT-EBSD experiment.

4 DISCUSSION

The microstructure of the martensitic stainless steel was in-situ investigated during a 1.5-hour tempering process at 500 °C. We observe two key changes in the microstructure.

The first effect is the growth of an oxidation layer during the restoration process of the matrix. During a heat treatment Cr diffuses from the carbides into the ferritic matrix and are replaced by Fe from the matrix [2]. Rosemann et al. performed Thermocalc calculation for carbide composition which shows at 500 °C that 10% of the mass in carbides is replaced by Fe at the expense of Cr. A Cr depleted zone at the interface between the carbides and matrix was present and insufficient chromium content in the metal matrix leads to unstable

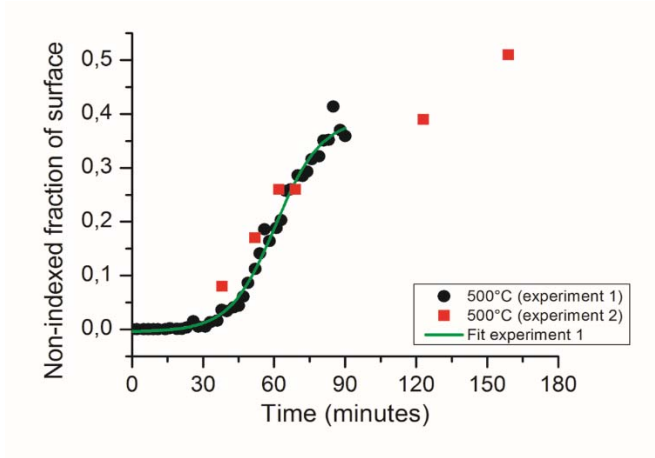

Figure 3: Non-indexable surface fraction as a function of the time. Main contributor of the non-indexability is the formation of an amorphous, oxide film during tempering. Surface oxidation rate is decreasing over time.

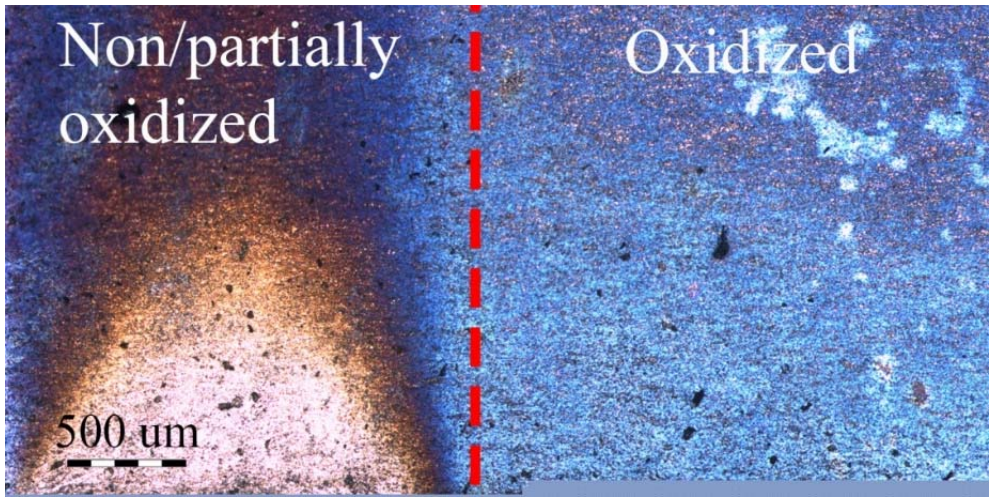

Figure 4: Optical image of sample surface after tempering. The right side of the surface is blue due to the creation of an oxide film during tempering. The left side was covered and therefore was (partially) protected against oxidation. This resulted in non (white) or partially (brown/blue) oxidized areas. The amorphous, oxide film degrades the quality of the Kikuchi pattern during the EBSD scan. After cooling the white areas are well indexable and the blue areas are not.

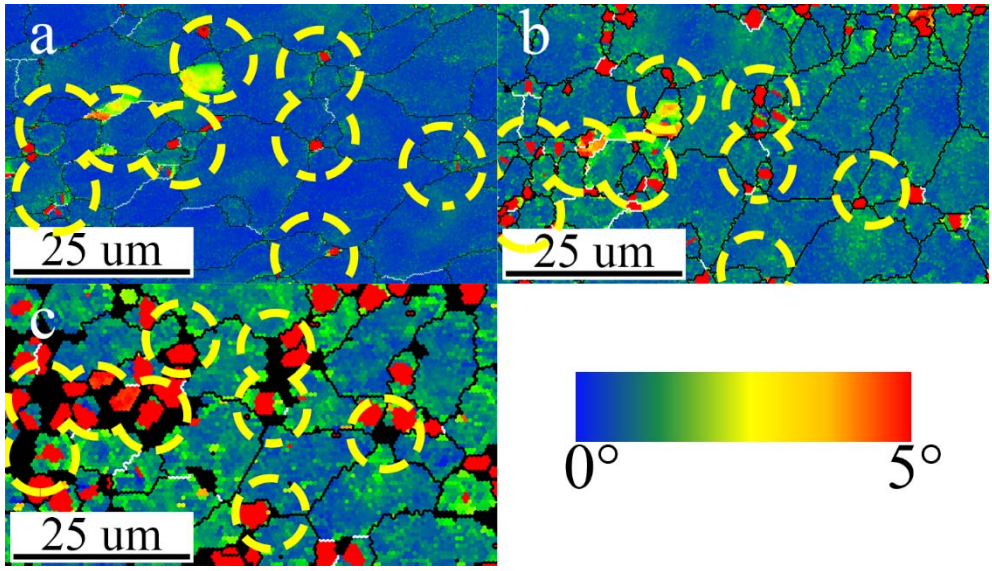

Figure 5: Kernel Average Misorientation maps of the global experiment. The 8th nearest neighbor was used for the construction of the maps. (a) is a map at RT before any temperature increase. (b) and (c) are maps respectively made 4 min and 52 minutes after reaching 500 °C. The maps show that sites with a high KAM at RT are preferred nucleation sites for oxidation (encircled in yellow).

formation of a passive layer and therefore a weak resistance to local corrosion [4]. Therefore, the relationship between temperature and carbide composition dictates the corrosion resistance as a function of the applied heat treatment.

From the microstructural observations, the preferred nucleation sites for oxidation can be inferred. The loss in Kikuchi diffraction pattern is attributed to the oxidation layer. A loss in Kikuchi pattern can have multiple reasons, e.g. high strain, non-crystallinity. In this case the oxidation layer is an amorphous layer exceeding thickness of few nm, which therefore gives no Kikuchi diffraction pattern. The locations which are non-indexable therefore correspond to the oxidized surface. The final oxidation layer is clearly visible at the end of the tempering process, Fig. 4. We expect mainly a chromium oxide layer, because the diffusion of Cr is faster than Fe at these temperatures [9]. However, we do not have definitive evidence.

The preferred oxidation sites have a high strain, Fig. 1. To see whether this is not only a local but also a global effect a larger area was scanned. In Fig. 5 the KAM map of an area at three stages are shown. For the construction of the maps the 8^{th} nearest neighbor is chosen for the KAM calculation. In Fig. 5(a) the map at room temperature is shown. Here we observe that the majority of the surface has a small amount of strain, however some locations and grains have a KAM larger than 2.5°. If we compare the map at RT with the map when the sample just reached 500°C in Fig. 5(b), the designated areas with high KAM at RT are similar. Finally, we compare it with the map after 52 hours and the positions of non-indexable points correlate well with the initial locations with high KAM at RT.

From Fig. 1 and Fig. 5 we conclude that locations with a high long-range strain are preferred sites for oxidation nucleation. This effect is observed at the local level as well as the global level. From the observations, the following mechanism is proposed. At the locally high strained locations it is easier for Cr to diffuse to the surface and for O to diffuse into the substrate, thereby increasing the probability of oxidation to start at that location. Initial strain already observed at RT designates these higher probabilities locations. Cr diffusion occurs preferentially through grain boundaries within the substrate and this remains the dominant path for diffusion until the path is obstructed by the continuous oxide growth [5]. On the other hand, the oxidation nucleation introduces locally extra crystallographic misorientation on the surface due to the addition of extra atoms. This in turn is beneficial for further oxidation nucleation: the oxidation rate therefore increases in the beginning with time as seen in Fig. 3.

The second effect is the increase in crystallographic misorientation. At this temperature, we are operating in the recovery regime of the material, because no nucleation of new grains was observed. Wawszczak et al. determined the recovery regime for ferritic steels at temperatures lower than 400°C and the recrystallization temperature for temperatures above 600°C, whilst calorimetric experiments show an exothermic peak at 500°C [10]. In the recovery regime, no changes in EBSD mapping and microstructure were observed, however during recrystallization there were modifications; recrystallization depend significantly on the stacking fault energy [10].

Recovery processes usually lead to loss of dislocation density or rearrangements to reduce the strain component, rearrangement of crystal lattices and stress relieve [1]. Because defects like dislocations are not in thermodynamic equilibrium a reduction in misorientation was expected. However, we observed the opposite effect in the case of stainless steel. The local average misorientation increased significantly, not only on the grain-boundaries but also in the interior of the grain, Fig. 1. The same effect is visible in the KAM distributions over time for both the short range as well as the long -range strain, Fig. 2. This means the crystallographic misorientation is increasing over time at 500 °C. An

explanation is that the recovery takes place in the bulk and dislocations glide escape to the surface. At the surface, they are locked or piled up due to the native oxide resulting in an increase of crystallographic misorientation near the subsurface layer. However, the increase in misorientation can also be an effect of the oxidation. This is still unclarified.

5 CONCLUSIONS

In this study, we observed in-situ the recovery process of martensitic stainless steel in the ferritic phase and correlated the oxidation nucleation to the microstructure of the material. We conclude the following:

- Loss of Kikuchi pattern is attributed to the growth of an amorphous oxidation layer.
- Locations with high KAM values are preferred locations for oxidation nucleation and are mainly in the neighborhood of grain boundaries and triple junctions.
- Preferred oxidation nucleation locations are already visible at RT by high KAM values.
- A general increase in crystallographic misorientation is observed at the surface during tempering of stainless steel.

ACKNOWLEDGEMENT

This research was carried out under the project number T63.3.12480 in the framework of the research program of the Materials innovation institute.

REFERENCES

[1] Humphreys, F.J. & Hatherly, M., *Recrystallization and related annealing phenomena*, **2**, Amsterdam; Boston: Elsevier, 2004.
[2] Rosemann, P., Kauss, N., Müller, C. & Halle, T., Influence of solution annealing temperature and cooling medium on microstructure, hardness and corrosion resistance of martensitic stainless steel X46Cr13. *Materials and Corrosion*, **66**(10), pp. 1068–1076, Oct. 2015.
[3] Rosemann, P., Müller, T., Babutzka, M. & Heyn, A., Influence of microstructure and surface treatment on the corrosion resistance of martensitic stainless steels 1.4116, 1.4034, and 1.4021. *Materials and Corrosion*, **66**(1), pp. 45–53, Jan. 2015.
[4] Müller, T., Heyn, A., Babutzka, M. & Rosemann, P., Examination of the influence of heat treatment on the corrosion resistance of martensitic stainless steels. *Materials and Corrosion*, **66**(7), pp. 656–662, Jul. 2015.
[5] Melfo, W.M. & Dippenaar, R.J., In situ observations of early oxide formation in steel under hot-rolling conditions. *Journal of Microscopy*, **225**(2), pp. 147–155, Feb. 2007.
[6] Lo, K.H., Shek, C.H. & Lai, K.L.J., *Recent developments in stainless steels*, 2009.
[7] Isfahany, A.N., Saghafian, H. & Borhani, G., The effect of heat treatment on mechanical properties and corrosion behavior of AISI420 martensitic stainless steel. *Journal of Alloys and Compounds*, **509**(9), pp. 3931–3936, Mar. 2011.
[8] Chakraborty, G. et al., Study on tempering behaviour of AISI 410 stainless steel. *Materials Characterization*, **100**, pp. 81–87, Feb. 2015.
[9] Langevoort, J.C., Sutherland, I., Hanekamp, L.J. & Gellings, P.J., On the oxide formation on stainless steels AISI 304 and incoloy 800H investigated with XPS. *Applied Surface Science*, **28**(2), pp. 167–179, Apr. 1987.
[10] Wawszczak, R. et al., Evolution of microstructure and residual stress during annealing of austenitic and ferritic steels. *Materials Characterization*, **112**, pp. 238–251, Feb. 2016.